JOURNAL OF GEOPHYSICAL RESEARCH, VOL. 99, NO. C6, PAGES 12,623–12,637, JUNE 15, 1994

Evaporation and solar irradiance as regulators of sea surface temperature in annual and interannual changes

W. Timothy Liu and Anzhen Zhang
Jet Propulsion Laboratory, California Institute of Technology, Pasadena

James K. B. Bishop[1]
Lamont-Doherty Earth Observatory, Palisades, New York

Abstract. Seven years of net surface solar irradiance (S) derived from cloud information provided by the International Satellite Cloud Climatology Project and 4 years of surface latent heat flux (E) derived from observations of the special sensor microwave imager were used to examine the relation between surface heat fluxes and sea surface temperature (T_s) in their global geographical distribution, seasonal cycle, and interannual variation. The relations of seasonal changes imply that evaporation cooling is significant over most of the ocean and that solar heating is the main drive for the change of T_s away from the equatorial wave guide where ocean dynamics may be more important. However, T_s is not the most direct and significant factor in the seasonal changes of S and E over most of the ocean; the solar incident angle may be more important to S, and wind speed and air humidity are found to correlate better with E. Significant local correlations between anomalies of T_s and S and between anomalies of T_s and E are found in the central equatorial Pacific; both types of correlation are negative. In this area, organized deep convection overlies the warm ocean, forms high clouds, and reduces S, while the low wind speed and high humidity that result from surface convergence reduce E. The negative correlation is not present in the surrounding areas where equally warm water and strong T_s anomalies are found under a subsiding atmosphere without similarly strong S and E anomalies. Correlation between anomalies of temperature tendency and the fluxes is weak, indicating that other factors are more influential in changing upper ocean heat balance during El Niño. The result shows that the relations between T_s and the flux components, in annual and interannual timescales, are not universal and not consistent with the local negative feedback postulations which require that an increase in T_s would result in an increase in local evaporative cooling and a decrease in local solar heating of the ocean. Large-scale atmospheric circulation changes clouds, winds, and humidity; they, in turn, influence the fluxes significantly. The influence of ocean dynamics in changing T_s in the tropical ocean can not be ignored.

1. Introduction

After numerical studies showed that global climate change is sensitive to small changes in sea surface temperature (T_s), considerable effort has been devoted to examining the role of surface fluxes in changing upper ocean heat balance and T_s, particularly in the tropical Pacific where interannual signals, such as the El Niño Southern Oscillation (ENSO), have major economic and ecological impacts [e.g., *Niiler and Stevenson*, 1982; *Leetmaa*, 1983; *Weare*, 1983; *Meyers et al.*, 1986; *Godfrey and Lindstrom*, 1989]. Studies in the past were hampered by a lack of basin-wide observations. In an attempt to overcome this undersampling problem, *Liu* [1988] and *Liu and Gautier* [1990] computed the two major components of surface thermal forcing, namely, latent heat (E) carried by evaporation and net solar irradiance from the sun (S), using satellite data. Their studies were confined to the central and eastern tropical Pacific, because the microwave radiometer data available at that time had geographically dependent errors and the geostationary Satellite GOES W had only limited coverage. The interest in the relation between surface heat fluxes and T_s, however, is not confined to the tropical ocean [e.g., *Cayan*, 1992]. Recent availability of satellite data from the International Satellite Cloud Climatology Project (ISCCP) and from the special sensor microwave imager (SSMI) on the operational spacecraft of the Defense Meteorological Space Program make it possible to derive E and S with adequate duration to study annual and interannual changes over global oceans.

Over global oceans, T_s rarely rises above 30°C, and a large area in the western Pacific and the east Indian Oceans, hereinafter referred to as the warm pool, has relatively uniform T_s between 28° and 30°C. Recently, *Ramanathan and Collins* [1991], hereinafter referred to as RC, found spatial correlation between local cloud forcing and T_s across the entire tropical Pacific and postulated that cirrus clouds

[1]Now at School of Earth and Ocean Sciences, University of Victoria, Victoria, Canada.

Paper number 94JC00604.
0148-0227/94/94JC-00604$05.00

are the main mechanisms in keeping local T_s at an equilibrium value and also in saving the Earth from runaway greenhouse warming. Their "thermostat hypothesis" led off renewed debates. K. E. Trenberth [*U.S. Congress*, 1992] argued that the feedback mechanism is not local; the ascending and descending branches of large-scale atmospheric circulation have opposing effects on cloud. *Wallace* [1992] suggested that the efficiency of large-scale circulation in redistributing the energy makes it unnecessary to have the cirrus cloud as a thermostat; uniform ocean temperature is just a reflection of uniform atmospheric temperature. *Fu et al.* [1992] also challenged the results of RC and, using observations from ISCCP, demonstrated that there is no cloud feedback when the data are averaged over the tropical Pacific; cloud forcing was controlled more by changes in large-scale atmospheric circulation than directly by local T_s. *Waliser and Graham* [1993] underscored the role of convection and they inferred, using satellite observations of outgoing longwave radiation and highly reflective cloud, that the highest sea surface temperatures are associated with reduced convection and cloud. The four studies, *U.S. Congress* [1992], *Wallace* [1992], *Fu et al.* [1992], and *Waliser and Graham* [1993], emphasized the importance of evaporation in regulating T_s, a process which was not considered important by RC.

Evaporation from the ocean has long been suggested as the mechanism responsible for the high cutoff in the frequency distribution of global T_s. The most common explanation is based on the nonlinear relation between temperature and saturation humidity, the Classius-Clapeyron function [*Fleagle and Businger*, 1963]. The capacity of the atmosphere in holding water vapor increases much more rapidly at high temperatures than at low ones. The inference is that evaporation will increase sharply with temperature over warm waters. The latent heat carried by evaporation cools the ocean and provides a negative feedback [*Priestley*, 1966]. In idealized conceptual studies [*Newell*, 1979] an equilibrium threshold T_s was derived by holding atmospheric wind speed, temperature, humidity, and irradiance constant and letting E rise rapidly with T_s. The efficiency in removing accumulated moisture in the atmosphere was not considered. The significance of the negative feedback of E on T_s has not been vigorously tested because of the lack of field observations.

In past studies on negative feedback, cloud forcing and convection were inferred from satellite observations of the top-of-atmosphere properties. The influences of convective ventilation and cloud cover on T_s must be manifested through surface fluxes of latent heat and radiation. Our main objective is to examine the relation between the two major surface heat flux components and T_s, making use of the SSMI and ISCCP data. The relations also provide an opportunity to check on the various postulations and analyses in the "thermostat debate", which are entirely based on annual and interannual variations.

2. Temporal Correlation to Be Tested

There are two common postulations related to the natural thermostat. Firstly, T_s has to be able to change the fluxes significantly, either through turbulence or convection, regardless of other conditions. Simply, any increase in T_s has to result in a decrease in S through an increase in cloud; that means a negative correlation between T_s and S. An increase in T_s should increase evaporation, which means a positive correlation between evaporation and T_s. On a monthly timescale, convection and turbulent transfer is fast and the correlation should be contemporary. The relation between E and T_s is known and, for all practical applications, can be represented by the bulk formula:

$$E = \rho_a C_E L u \Delta q \tag{1a}$$

$$\Delta q = q_s - q_a = [Q(T_s) - rQ(T_s + \Delta T)] \tag{1b}$$

where C_E is the transfer coefficient, r is the relative humidity, ρ_a is the air density, L is the latent heat of vaporization, u is the wind speed, q is the specific humidity, T is the potential temperature, ΔT and Δq are the sea-air temperature and humidity differences, $Q(T)$ represents the saturation specific-humidity as a function of temperature T, subscript s represents the value at the sea-air interface, and subscript a represents the value at a reference level in the atmospheric constant flux layer (approximately 50 m thick). E would increase with T_s at a rate governed by the CC function, only if u, ΔT, and r are relatively constant. If the u and q_a effects are stronger, there will be positive correlation between u and E, and negative correlation between q_a and E. All these correlations will be examined later.

Secondly, the fluxes should have significant impact on changing T_s through upper ocean heat balance. The importance of various terms in the upper ocean heat balance at various locations and seasons has been extensively studied through observation and modeling. A simplified representation of the heat balance in a well-mixed layer of the upper ocean of depth h with temperature approximately equal to T_s is

$$\rho_w c h \frac{dT_s}{dt} = S - E + A + B \tag{2}$$

where t is the time, ρ_w is the water density, and c is the isobaric specific heat of water. A represents both vertical and horizontal heat transported (by advection, turbulence, and diffusion) into this layer. The sum of sensible heat flux and longwave radiation at the surface and the radiation penetration through the bottom of the mixed layer are represented by B. If E is dominant relative to other terms on the right side of (2), and if h is relatively constant, there should be a significant negative correlation between E and temperature tendency dT_s/dt. On the other hand, if S is more important, there should be a positive correlation between S and dT_s/dt. Over most of the ocean, the annual cycle of T_s is sinusoidal and dT_s/dt is 90° off phase. That means we could replace the tendency with lag T_s and get the same correlation. It takes time to warm up the mixed layer.

We should be able to shed some light on the causes and effects of T_s changes by examining simultaneous and lag correlations. The temporal relation between T_s and fluxes in seasonal cycles and in ENSO anomalies will be examined in sections 6 and 7.

3. Data and Flux Computation

The basic method of computing E from satellite data was described and validated by *Liu* [1988]. According to (1), the estimation of E requires the knowledge of C_E and the

measurements of u, q_a, and T_s. In this study, C_E is determined by a surface layer turbulent transfer model which accounts for the transition from rough flow (moderate and high winds) to smooth flow (low winds) and the moisture-induced atmospheric density stratification [*Liu et al.*, 1979]. In this model, C_E is roughly equal to 1.3×10^{-3} [cf. *Friehe and Schmitt*, 1976], increases sharply with decreasing wind when $u < 2$ m/s, and decreases slightly at high winds. Recently, the high wind characteristic of the model was supported by measurements in the North Sea [*Katsaros and DeCosmo*, 1993] and the low wind characteristic was found to be in excellent agreement with field measurements in the Bismarck Sea [*Bradley et al.*, 1991]. The transfer coefficient depends on atmospheric density stratification, which is affected by air temperature. Air temperature used in the computation of E was derived from q_a with the assumption of $r = 80\%$. The error in E introduced by this assumption is relatively small since air temperature has only a secondary effect through stability of the atmosphere. The validity of using monthly parameters instead of instantaneous measurements in this model was tested in subtropical and temperate oceans using time series from weather ships [*Esbensen and Reynolds*, 1981]. The errors due to the neglected high-frequency variance are found to be small. This is in agreement with studies using continuous in situ measurements at two locations in the equatorial Pacific, one in the cold tongue in the east and the other at Truk Island in the convective region of the warm pool [*Liu*, 1988]. Large variances have been observed during short-period, small-scale, and intermittent convections in the warm pool [e.g., *Young et al.*, 1992], but there has not been any quantitative evaluation of the impact of these high-frequency and small-scale variances on large-scale and monthly means to support or dispute the results of *Liu* [1988] and *Esbensen and Reynolds* [1981], because there is no long-duration measurement of high temporal resolution.

Spaceborne sensors can measure u and T_s but not q_a. A spaceborne microwave radiometer can measure the column integrated water vapor (W) accurately. The method to estimate E from satellite data is anchored on the feasibility of estimating q_a from W. The main rationale of relating q_a to W is the decoupling of the dominant mode of variability in humidity profiles, which is coherent through the entire atmospheric column from other modes, which are coherent only through limited depths [*Liu et al.*, 1991]. For periods longer than two weeks, W is a good estimator of the humidity profiles and q_a. Other factors governing q_a variability, such as boundary layer changes, are important largely for shorter periods. A global relation between monthly q_a and W was derived using 17 years of radiosonde reports from 46 ocean meteorological stations [*Liu*, 1986]. The empirical relation was tested, using soundings from field experiments, routine ship reports, and atmospheric general circulation models [*Liu*, 1988; *Hsu and Blanchard*, 1989; *Liu et al.*, 1992]; it was found sufficiently accurate to describe the annual and interannual variabilities. However, systematic errors were found in the western North Pacific and North Atlantic and off the coast of Baja California during three summer months, resulting in overestimation of q_a [*Liu*, 1986; *Liu et al.*, 1992]. The resultant stable stratification causes spurious suppression of turbulent transport and failure of the *Liu et al.* [1979] model. There are continuous efforts to evaluate this relation but the work is handicapped by a lack of accurate humidity measurements over extensive areas of the ocean. For example, humidity climatologies are found to smear out the sharp gradients on the eastern tropical and subtropical southern oceans where in situ measurements have been extremely sparse [*Liu et al.*, 1992].

The data set for this study consists of u and W from SSMI which were averaged into monthly fields with 1° latitude by 1° longitude resolution. The T_s data used are based on advanced very high resolution radiometers (AVHRR) observations, blended with available in situ measurements [*Reynolds*, 1988]. The T_s fields were spatially interpolated to SSMI grid positions using a Lagrangian interpolator [*Press et al.*, 1989] before computing E. This data set provides coverage over the global ocean for 47 months from July 1987 to June 1991, with December 1987 data missing. The period includes part of the warm phase and the entire cold phase of an ENSO episode. The Multichannel Sea Surface Temperature (MCSST) data products from AVHRR [*McClain et al.*, 1985] were also tested. This data set has higher temporal and spatial resolutions than the blended data but was found to include large deviations (from surrounding values) at high latitudes and therefore was not used in this study.

Cloud is the most serious uncertainty in the derivation of S. The techniques of retrieving S make use of the high sampling rate and high resolution of visible and infrared sensors on geostationary satellites. Global coverage requires data from five geostationary satellites run by four national agencies, with uncalibrated data in various formats. The task was forbidding until ISCCP set up the protocol for international data exchanges and provided calibrated standard products for the users [*Rossow and Schiffer*, 1991]. The method for computing S was described by *Bishop and Rossow* [1991]. Parameters from the renormalized ISCCP C1 data set, including solar zenith angle, atmospheric water vapor profile, ozone column abundance, cloud fraction, cloud optical thickness, visible surface reflectance, surface type, and surface pressure, were used to derive both clear and cloudy components of the radiance, at 2.5° latitude by 2.5° longitude and 3-hour resolution, using a set of simplified radiative transfer equations. A daily sampling correction factor was applied to the sum of the two components to form daily values. Six percent of the downwelling solar flux was assumed to be reflected back. Monthly means from July 1983 to June 1990 interpolated to SSMI grid locations were used in this study.

4. Ensemble Relation

Scatterplots of the ensemble of data have been commonly used to demonstrate the hypothesis on local feedback [e.g., RC; *Waliser et al.*, 1993]. The ensemble of data in the form of average S and E as functions of T_s is shown in Figure 1. The top and bottom panels of the figure are produced by averaging all the values of S and E within each T_s bin of 0.5°C for 84 and 47 months, respectively. Data with $T_s <$ 0°C, from areas poleward of 60° latitudes, and from enclosed seas (e.g., Persian Gulf and Red Sea) are excluded. In the figure the standard deviations are shown as error bars and the numbers of data in the bins are also plotted on logarithmic scales. At low T_s the fluxes are positively correlated with T_s. After E peaks at 25°C and S at 26°C both fluxes decrease with increasing T_s. Above 29°C, S clearly increases with T_s again. The two transitions in gradients

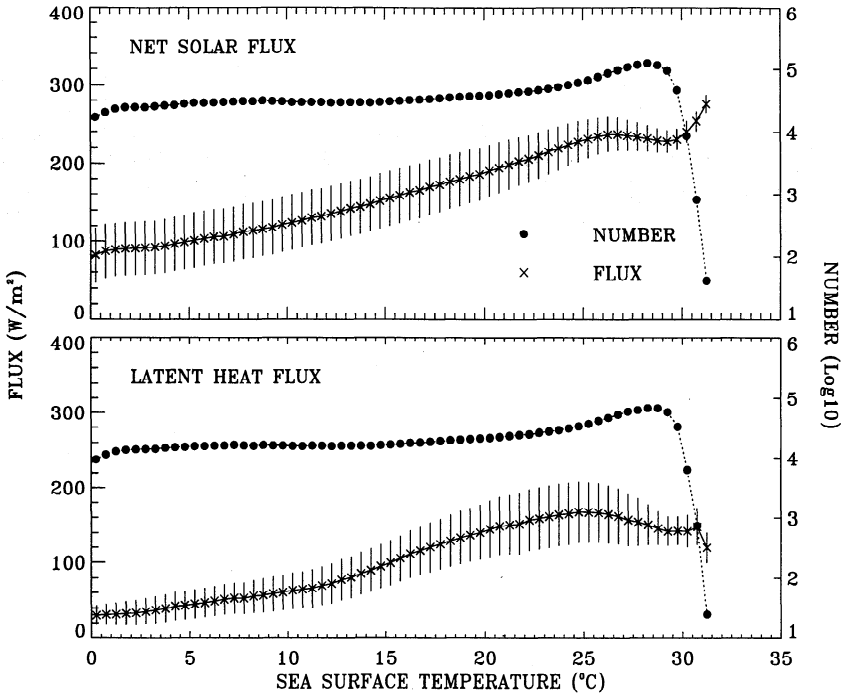

Figure 1. (top) Bin-averaged net solar flux and (bottom) latent heat flux as functions of sea surface temperature, for 0.5°C sea surface temperature bins, with standard deviations (error bars) and population of the bins also shown.

roughly coincide with those of convective activities derived from satellite observations of outgoing longwave radiation as a function of T_s by *Waliser et al.* [1993]. Their study shows that the correlation between convective activities and T_s is positive when 26.5°C < T_s < 29.5°C but negative when T_s > 29.5°C.

The positive gradients at lower temperatures (T_s < 26°C) in Figure 1 may reflect the general tendency for evaporative cooling and solar heating to increase toward low latitudes. When 26°C < T_s < 29°C, the warm ocean provides adequate moist static energy for the ascent of saturated air parcels from the surface into deep convection [e.g., *Betts and Ridgway*, 1989]. The increase of convection within this range of warm temperature has been observed by *Gadgil et al.* [1984], *Graham and Barnett* [1987], and others. The increase in cloud cover associated with deep convection reduces solar heating. Similar negative correlation forms the basis of the hypothesis of RC. In this range of T_s, E does not increase with T_s according to the CC formula. The decrease of E with increase in T_s is in agreement with monthly mean and ENSO anomalies observed by *Liu* [1988] and the climatological distribution of E and T_s. *Liu* [1988] suggested that the high q_a and low u (convergence) in the center of organized convection or under the ascending branches of the Hadley and Walker circulation cause lower evaporation. At high temperature (T_s > 29°C), S increases with increasing T_s, contrary to the local feedback postulation of RC. *Waliser et al.* [1993] examined the high T_s carefully and concluded that in the case of subsidence over a warm ocean, suppression of cloud formation allows for the increase in S and T_s. E also increases slightly with T_s at the high temperatures. The exception is the point at T_s = 31°C, which is derived from drastically less data and which may be in error. Dry and subsiding air may be the reason for the slight increase of E with T_s, even over warm water. Figure 1 shows that both E and S are positively correlated with T_s at low temperature, but the correlations turn negative at high temperature. However, this behavior is not universal and it breaks down as we separate the geographical from temporal variations.

5. Geographical Variability

Ensemble scatterplots like Figure 1 do not distinguish the relation in temporal and spatial variabilities, nor do they reveal any remote relationship linked by circulation. To compare geographical variability, the distributions of monthly S, T_s, and E for a typical boreal summer month (July 1989) and for a typical boreal winter month (January 1990) are compared in Plate 1. The missing data in the North Pacific and North Atlantic shown in the July E map (lower left) are the consequences of the $q_a - W$ model failure discussed in section 3. It is obvious from the figures that high T_s do not always correspond to high E and low S, as would be expected from the hypotheses of negative feedback. In a zonal belt just north of the equator marking the approximate position of the Intertropical Convergence Zone (ITCZ), in a region running southeast from Indonesia corresponding to the South Pacific Convergence Zone (SPCZ), and over the warm pool, E is relatively low where the highest T_s are found. High E is located in the trade wind regions of the winter hemisphere but T_s in not the highest. The high evaporation south of Japan during winter months may reflect the dry continental air as much as the warm water of Kuroshio. Positive relation is only found in the eastern tropical ocean basin where the cold water from upwelling reduces evaporation. The distribution is consistent with climatology derived from ship reports [e.g., *Weare et al.*, 1981; *Hsiung*, 1986] with low E in the ascending branch of

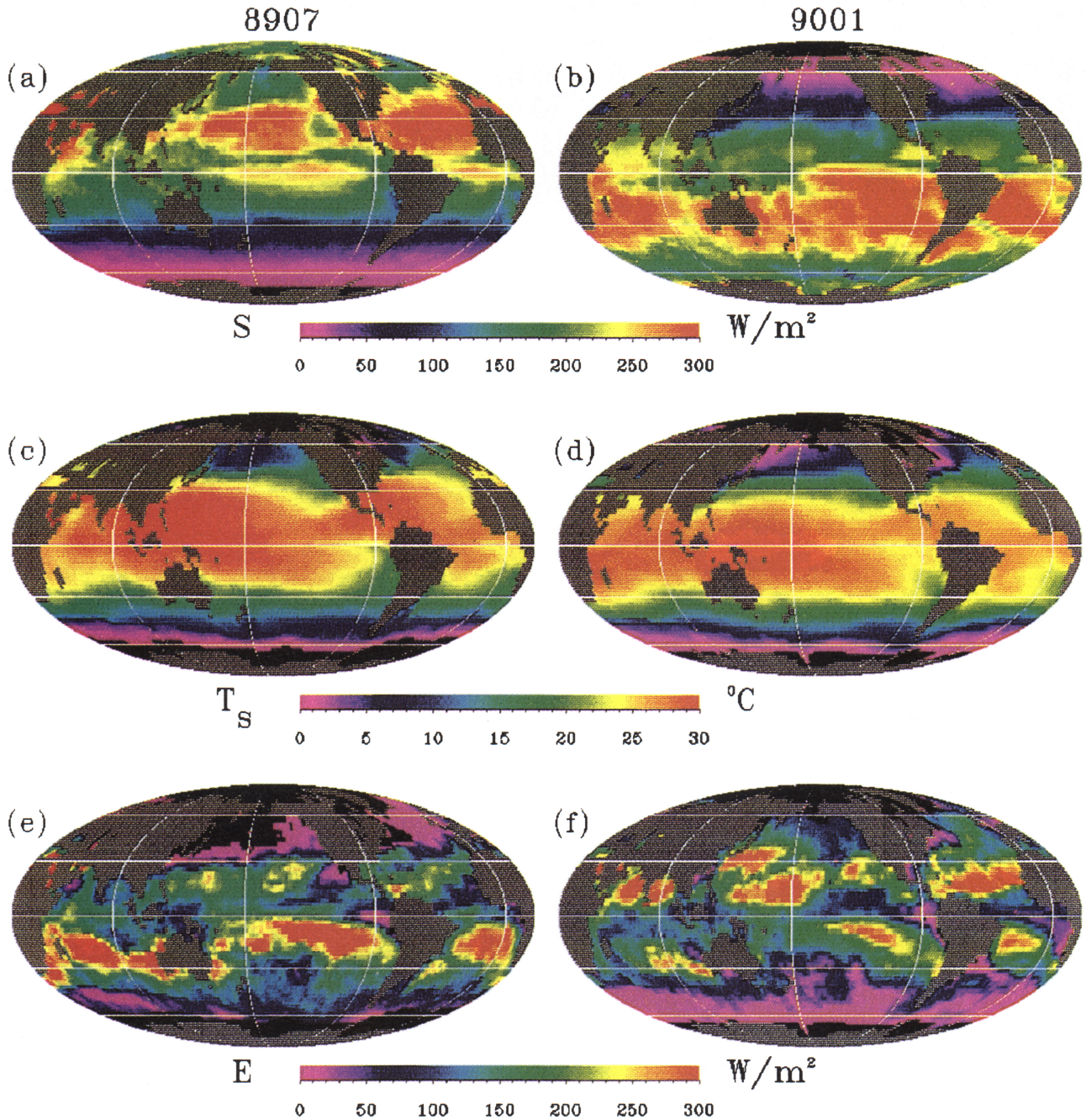

Plate 1. Monthly means of net solar flux for (a) July 1989 and (b) January 1990. Sea surface temperature for (c) July 1989 and (d) January 1990. Latent heat flux for (e) July 1989 and (f) January 1990. Left side and right side are typical of boreal summer and winter, respectively.

the Hadley and Walker circulations and high E in the descending branch and trade wind regions. The low values of E found in areas of high T_s were noticed by a few investigators [e.g., *Cornejo-Garrido and Stone*, 1977; *Liu*, 1990; *Ramanathan and Collins*, 1993]. The solar flux shows much stronger seasonal migration than T_s. Besides the major meridional variation, which is governed by seasonal change of solar incident angle, high S is found in regions of subsidence and clear sky and low S is found in ascendance and convection; such a relation to atmospheric circulation is not obvious in T_s distribution.

The distributions of anomalies in two typical months during the warm and cold phases of ENSO are shown in Plate 2. The anomalies are formed by removing the 'climatological' annual cycle from the monthly means. The climatological annual cycles of various parameters are formed by averaging the parameters of each calendar month for the entire period in which data are available. Limited by data availability, the 'climatologies' of E and S are formed from different lengths (4 and 7 years, respectively) of data which do not completely overlap. Rather than using different T_s climatologies for comparison with E and S, a single T_s climatology derived from 9 years (January 1982–December 1992) of data was used, and the T_s anomalies discussed

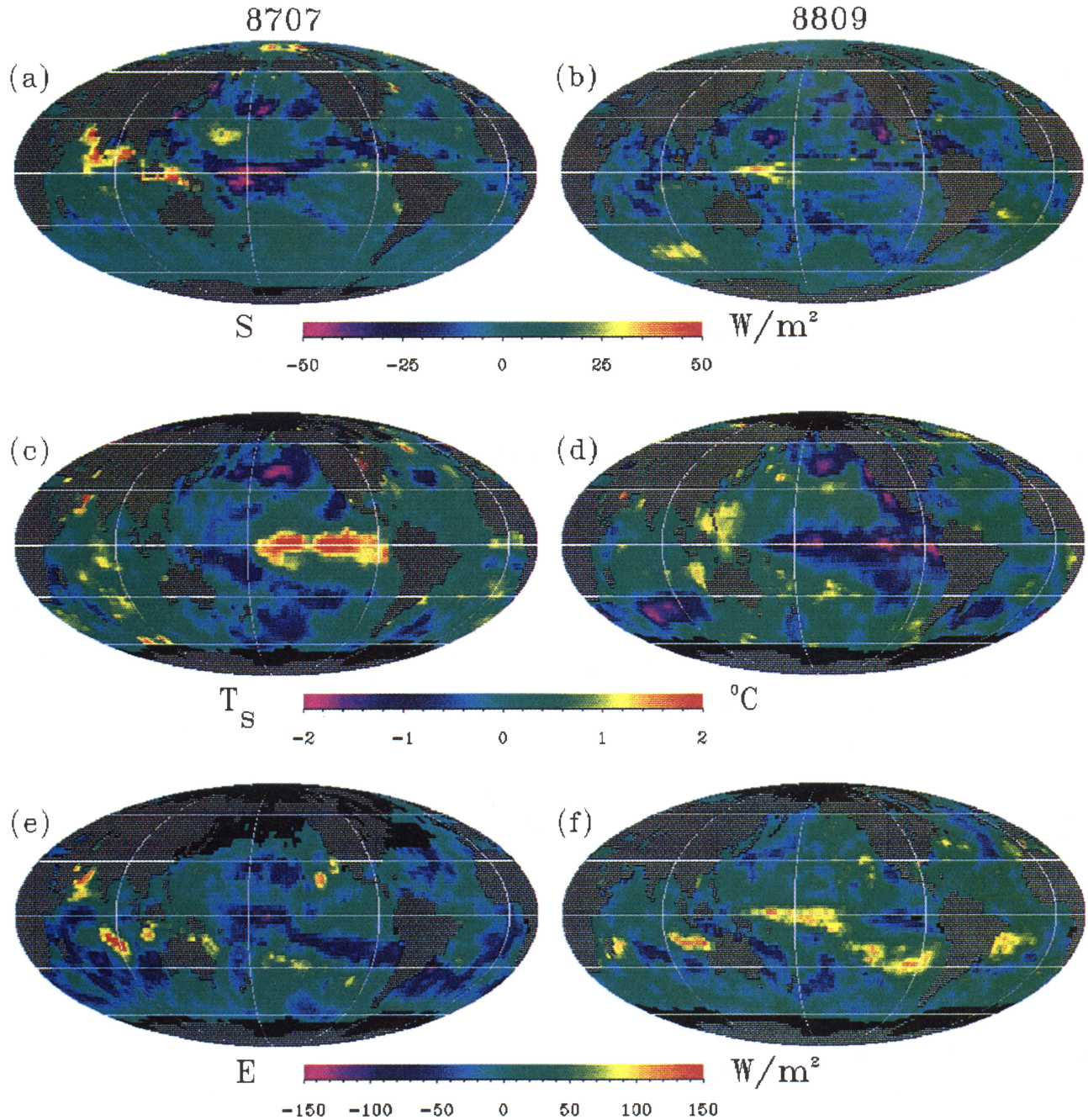

Plate 2. Anomalies of net solar flux for (a) July 1987 and (b) September 1988, sea surface temperature for (c) July 1987 and (d) September 1988, and latent heat flux for (e) July 1987 and (f) September 1988, during the warm and cold phases of an El Niño Southern Oscillation episode.

hereinafter are based on this common climatology. As shown in Plates 2a and 2b, significant positive and negative S anomalies are found in the central equatorial Pacific, roughly where warm and cold T_s anomalies are also found (Plates 2c and 3d), although the peaks of S anomalies are displaced to the west of T_s peaks. However, in the eastern equatorial Pacific where equally large T_s anomalies are found, no large S anomalies are observed. The displacements of S anomalies from T_s anomalies, which have been observed from outgoing longwave radiation, are likely to result from atmospheric dynamic response to surface heating, and the local feedback postulation is not sufficient to explain the relation between cloud and T_s. As with the monthly means, negative E anomalies in the central equatorial Pacific (Plates 2e and 2f) are associated with positive T_s anomalies and vice versa, contrary to the negative feedback hypotheses. The centers of E anomalies are also displaced slightly to the west of the center of T_s anomalies. In the eastern equatorial Pacific, E anomalies are weak in July 1987 despite large T_s anomalies. However, negative anomalies are found over significant negative T_s anomalies in September 1988.

No simple universal relation between the geographical distribution of surface fluxes and T_s, either for the monthly

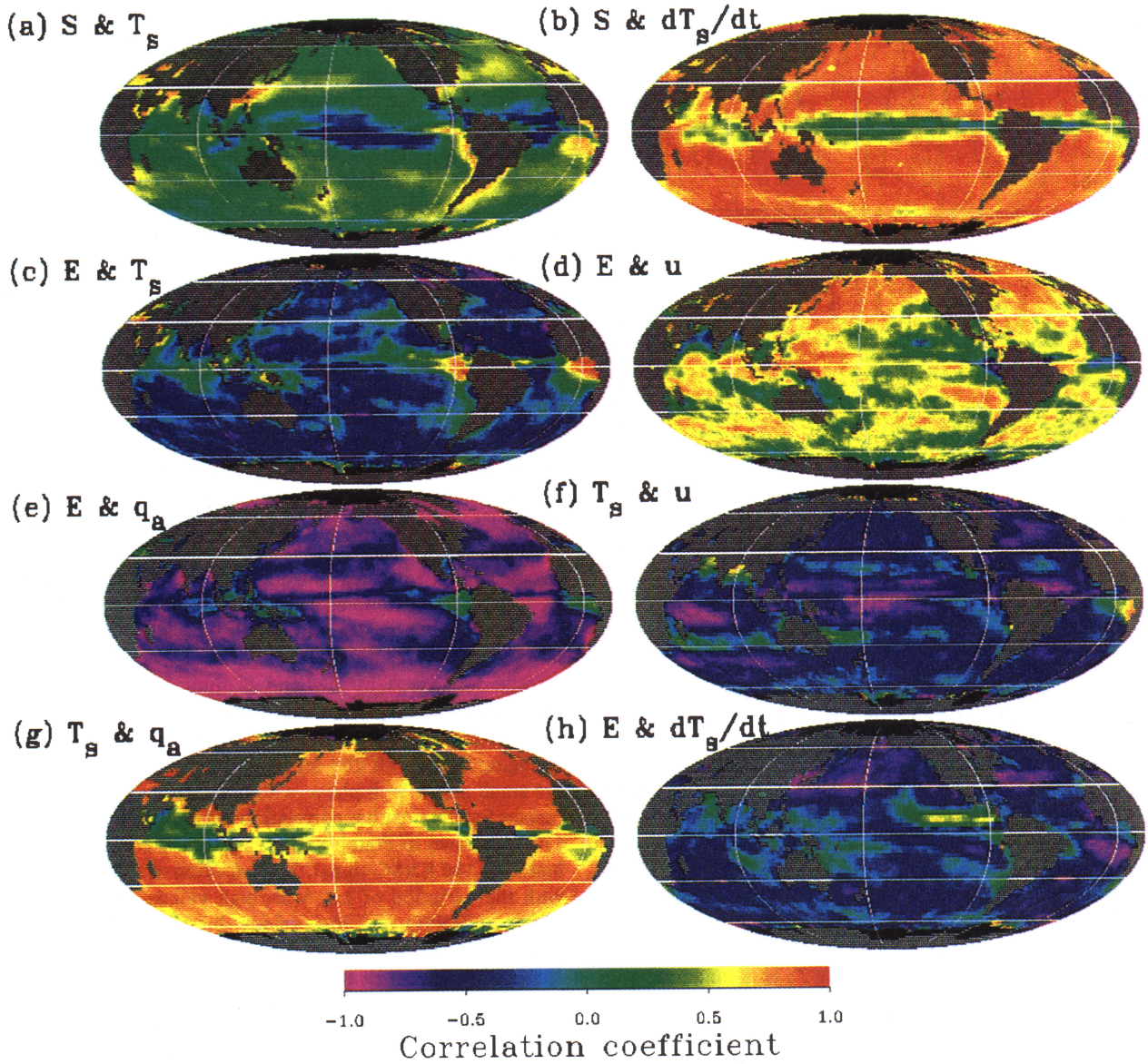

Plate 3. Correlation coefficients between various monthly-mean parameters. (a) S and T_s; (b) S and dT_s/dt; (c) E and T_s; (d) E and u; (e) E and q_a; (f) T_s and u; (g) T_s and q_a; and (h) E and dT_s/dt.

means or for the anomalies, is evident. It is interesting to note that while the ranges of monthly means are similar for E and S, the range of E anomalies is much larger than the range of S anomalies, as noticed by *Fu et al.* [1992].

6. Seasonal Cycle

To examine the relation of temporal variabilities between the fluxes and T_s, the distribution of correlation coefficients is used. While the correlation coefficient is simple to understand, it may not fully represent the nonlinear relationship between two variables. As a test the explained variances of high-order polynomial regressions were selectively examined, but their patterns were largely similar to those of linear correlation coefficient and are not shown. Away from the equator the monthly variation is dominated by the seasonal cycle. The monthly correlations between S and T_s and between S and dT_s/dt, shown in Plates 3a and 3b, clearly reveal the cause and effect of seasonal T_s changes. For 84 pairs of independent data a correlation higher than 0.28 would be significant at a 99% level. In reality, not all the data are independent and the correlation coefficient has to be higher than 0.28 to be significant. Plate 3a shows that except in the near-equatorial oceans where interannual changes are important, there is no significant negative correlation between S and T_s. As we would expect, T_s does not drive the seasonal change of S, which depends largely on solar incident angle. However, the correlations between S and dT_s/dt are significantly positive everywhere except in a narrow strip along the equator across all of the three oceans (Plate 3b). The distribution is almost identical when dT_s/dt is replaced by T_s with a 3-month lag.

The seasonal change of T_s is largely driven by S, away

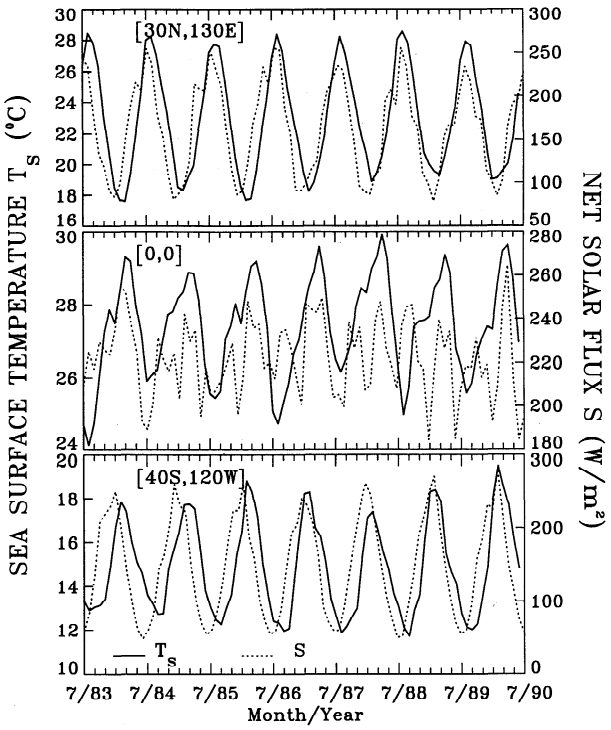

Figure 2. Time series comparison of monthly mean net solar flux and sea surface temperature at selected locations.

from the equator. The annual cycles of S and T_s are clearly seen at 30°N, 130°E and 40°S, 120°W (shown in Figures 2a and 2c) with S reaching a high value during summer and a low value during winter. S leads T_s by a few months and therefore is in phase with dT_s/dt. This is the reason for the high positive correlations. At the equator and 0° longitude, in the equatorial waveguide, ocean dynamics is more important in governing the change of T_s. While T_s is dominated by the Austral annual cycle, the semiannual period is predominant in the variation of S, as shown in Figure 2b. The results are consistent with those by *Liu and Gautier* [1990], using different sets of satellite data covering a different period of time.

The distributions of correlation coefficients between E and T_s are shown in Plate 3c. For 47 independent pairs of data a correlation coefficient higher than 0.39 would be significant at a 99% level. Significant positive correlations are found only in the eastern equatorial Pacific and Atlantic near the coasts. These areas are relatively small. Over most of the ocean, there is no significant positive correlation. The negative correlation between E and T_s, found over most of the ocean, is perhaps caused by a third factor. This factor could be u, which correlates positively with E (Plate 3d) but negatively with T_s (Plate 3f), or q_a, which correlates negatively with E (Plate 3e) but positively with T_s (Plate 3g). The implication is that, over large areas of the ocean, T_s is not the most direct factor in the seasonal change of evaporation. Atmospheric parameters that have higher variabilities are more important in governing the seasonal changes of E. In the eastern equatorial Pacific and Atlantic, the correlations between E and u are negative and the correlations between E and q_a are weak; the variability of E is dominated by T_s. Over the warm pool in the western Pacific and eastern Indian oceans the correlations between E and T_s and between E and q_a are both weak; the variation of E is dominated by u. The distribution of correlation coefficients between E and dT_s/dt is shown in Plate 3h. The distribution is almost identical with the correlation between E and lag T_s (not shown). Over most of the ocean the correlations are largely negative and relatively strong in midlatitudes. Evaporation appears to provide important seasonal cooling of the upper ocean. The exception is in the eastern Pacific just north of the equator where an unexplained zonal band of positive correlation is found.

To elucidate the correlation between E and T_s, time series at six selected locations are shown along with those of u and Δq in Plate 4. At 40°N, 160°E and 40°S, 40°E the annual cycles of E are in phase with u and Δq, with lows in summer and broad peaks in winter, in agreement with (1). They are roughly 90° (3 months) out of phase with T_s, which peaks in late summer or autumn. The highs of E are roughly 3 months ahead of the lows in T_s. Since T_s variation is dominated by the annual cycle (away from the equatorial region) and has a 3-month phase difference with dT_s/dt, E has strong negative correlation with the temperature tendency. In the eastern Pacific and Atlantic near the equator, the influence of wind is weak, and two examples are shown in Plate 4. At 10°S, 0° a phase difference between E and T_s, similar to that at higher latitude, is found, but here the annual cycle of E is completely dominated by Δq and is quite different from the temporal variability of u. At this location the annual range of u is relatively small and u does not play an important role in changing E. At 0°, 0° the seasonal variation of both u and q_a are small and E is in phase with both Δq and T_s; this is the reason for the positive correlation between E and T_s. At 0°, 170°W, shown in Plate 4e, the variation is completely dominated by the ENSO signal. The variation of E agrees closely with the variation of Δq, with high values during the cold phase of ENSO and low values during the warm phase; negative correlations are the result. Over the warm pool 0°, 150°E, there is no clear annual cycle and the variation of E agrees best with u. The dominant influence of wind on the variation of E was suggested by *Liu* [1988] and is supported by in situ observations [e.g., *Meyers et al.*, 1986; *McPhaden and Hayes*, 1991].

The time series comparisons show that the main factor governing E varies with location; T_s is the dominant factor only over a very limited area, and the influence of u and q_a can not be discounted. Over most of the ocean, high T_s does not coincide with high E. The important role played by evaporative cooling in upper ocean heat balance is a probable reason for the negative correlations between E and temperature tendency. Other possible explanations are discussed in section 8.

7. ENSO Anomalies

The correlation coefficients for colocated and contemporary anomalies are shown in Plate 5. The most striking features are the negative correlations between S and T_s (Plate 5a) and between E and T_s (Plate 5c), in the central equatorial Pacific, with a weak eastward extension north of the equator and a strong extension toward the southeast. These strong local correlations are found in areas of significant flux anomalies during ENSO (see Plate 3). The negative correlations between the anomalies of S and T_s were observed by *Liu and Gautier* [1990], *Chertock et al.* [1991], and

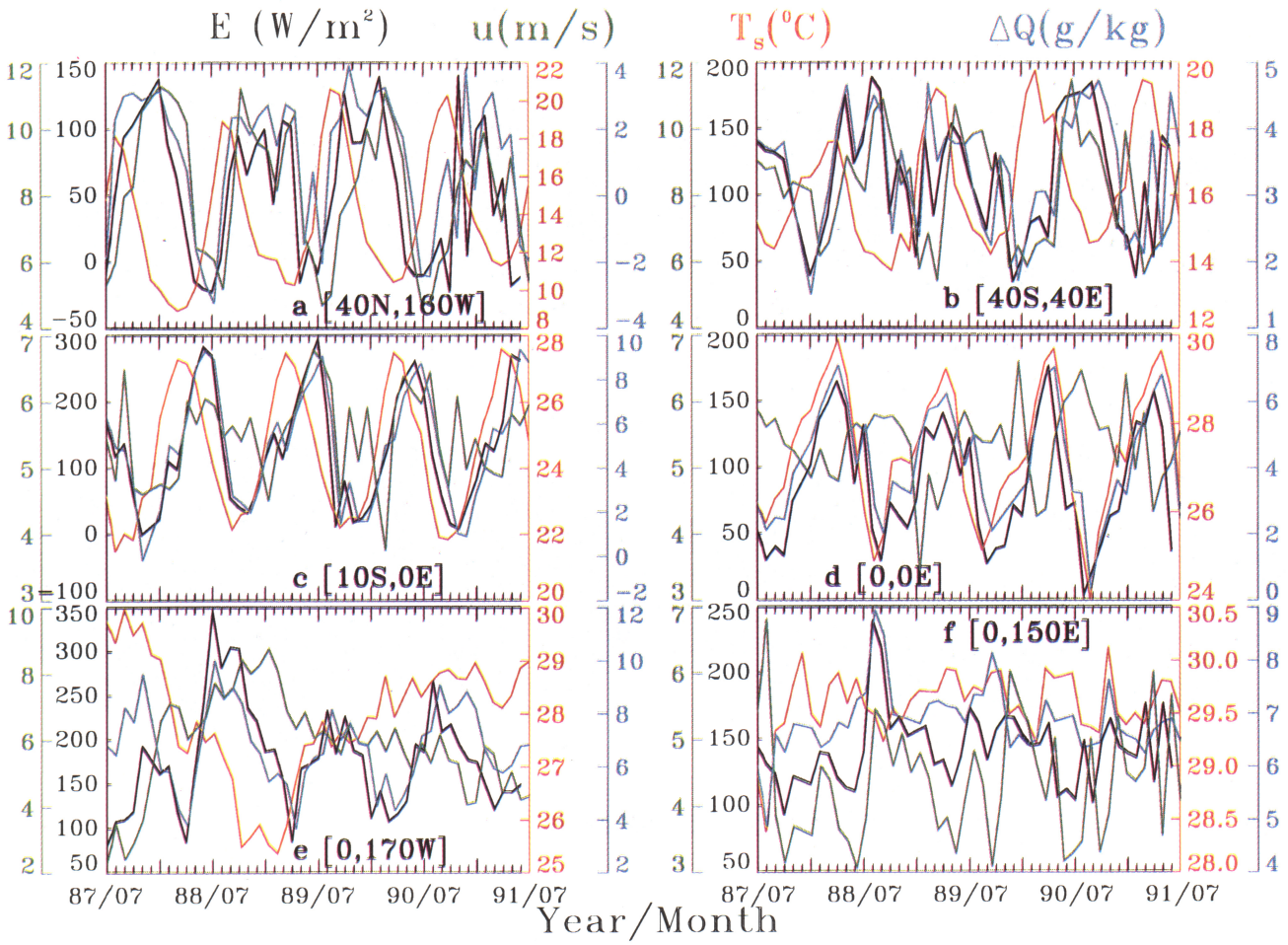

Plate 4. Time series comparison of monthly mean latent heat flux (black line), sea surface temperature (red line), wind speed (green line), and sea-air humidity difference (blue line) at (a) 40°N, 160°W; (b) 40°S, 40°E; (c) 10°S, 0°E; (d) 0°, 0°E; (e) 0°, 170°W; and (f) 0°, 150°E.

others before. They suggest that S anomalies are, perhaps, influenced by local T_s through cloud, as articulated by RC. However, the relation is not universal and does not hold in some surrounding areas with equally warm water or significant T_s anomalies but with no significant S anomalies. The results support the argument that cloud and S anomalies are more directly linked to large-scale circulation than local T_s. The lack of significant positive correlation between S and dT_s/dt (Plate 5b) suggests an anomalous S has a weak influence in the anomalous change in T_s relative to other factors in (2), in agreement with *Liu and Gautier* [1990]. Some positive correlations between S and dT_s/dt are found in the subtropical oceans where T_s anomalies are weak, but they may not be significant.

Positive correlations between anomalies of E and T_s are found only in the eastern equatorial Pacific and Atlantic, as shown in Plate 5c. In the central equatorial Pacific the negative correlations between E and T_s again suggest that evaporation is not directly driven by local T_s, even in interannual timescales. Above-normal T_s is found in the same places as lower than normal evaporation and vice versa, in agreement with *Liu* [1988] based on different sets of data during different ENSO episodes. The variability of other factors, such as u and q_a, must be taken into consideration. There are significant negative correlations between E and the temperature tendency (Plate 5d), in agreement with *Liu and Gautier* [1990], albeit weaker than expected. E appears to have a stronger influence on anomalous T_s change than does S.

Significant negative correlations are found in the regions where organized deep convection or the ascending branch of the Walker Circulation was displaced during ENSO but are not found over the descending branch of large-scale circulation, indicating the importance of large-scale atmospheric circulation. Ascending air has to be compensated for by descending air with an opposite effect on the fluxes, probably over equally warm water. To examine the role of large-scale circulation, the interannual anomalies of S, E, and T_s averaged over areas encompassing various parts of the Hadley and Walker circulations are compared in Figures 3 and 4. In Figures 3a and 4a the parameters are averaged over the central equatorial Pacific, 5°N to 5°S and 170°E to 130°W, where the ascending branch was displaced during the 1987–1988 ENSO. They clearly show a negative correlation during the ENSO event. The correlation coefficients are −0.76 between the time series in Figure 3a and −0.63 between the time series in Figure 4a. The S anomalies during both the warm and cold phases of the 1987–1989 ENSO are largely eliminated as the averaged area is expanded (30°N to 30°S, 90°E to 80°W) to include the descending branch of the

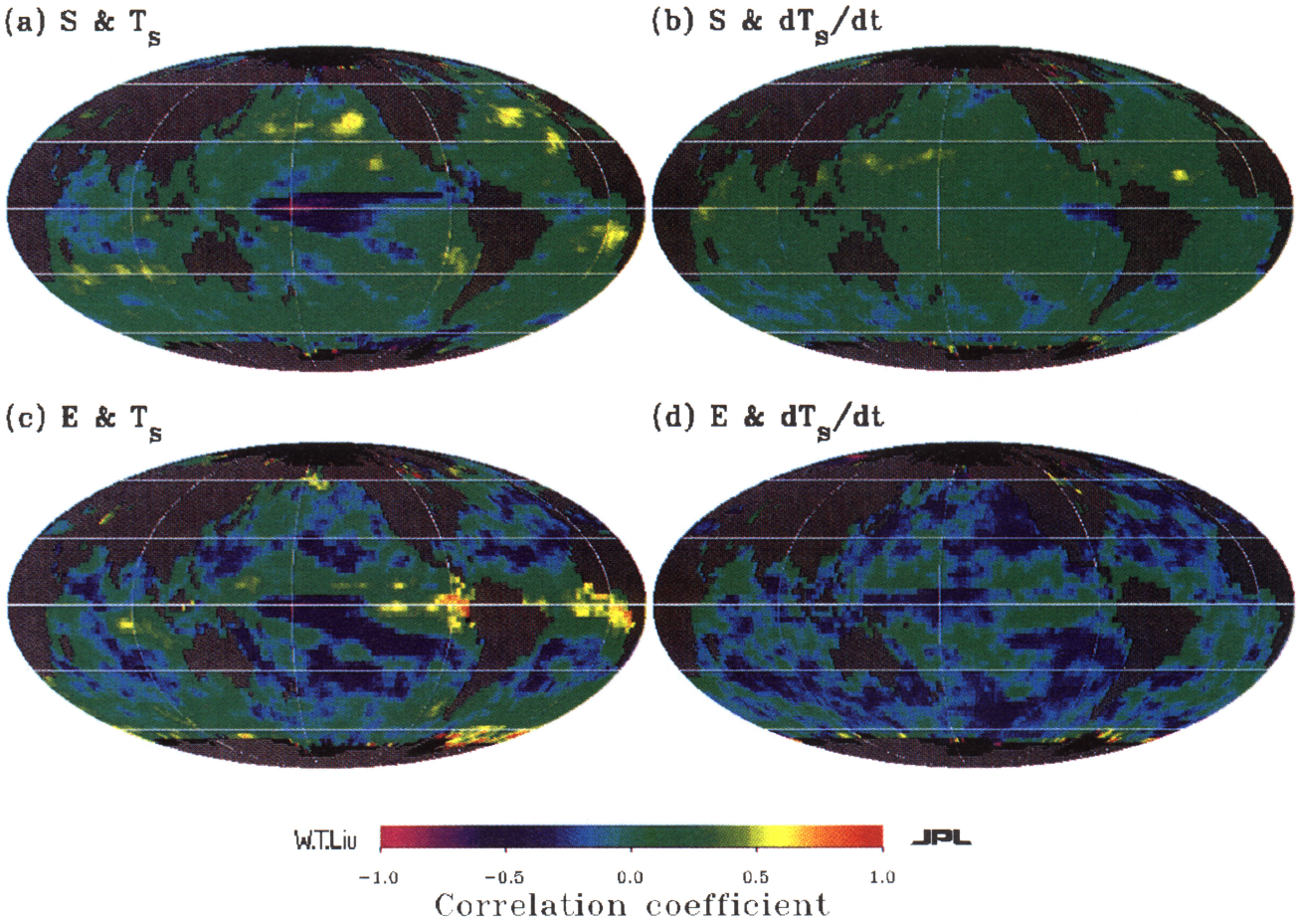

Plate 5. Correlation coefficients between anomalies of (a) solar flux and sea surface temperature; (b) solar flux and temperature tendency; (c) latent heat flux and sea surface temperature; and (d) latent heat flux and temperature tendency.

circulations (Figure 3b), perhaps because S anomalies in ascending and descending branches cancel each other, as suggested by *Fu et al.* [1992]. The time series in Figure 3b have a correlation coefficient of −0.02 which is not significant. On the other hand, the E anomalies are preserved, although over a shorter period (Figure 4b). Although the large negative and positive E anomalies in August 1978 and August 1988 correspond to positive and negative T_s anomalies, respectively, the correlation coefficient of −0.14 between the two time series is rather insignificant. The time series in Figures 3c and 4c are averaged over the same area as Figures 3b and 4b, but only data with $T_s > 29$°C are used. There are no large S anomalies during the warm and cold phases of ENSO, and the correlation coefficient of −0.04 between the S and T_s time series in Figure 3c is insignificant. Over the warm water the anomalies of E and T_s are opposite of each other, with a correlation coefficient of −0.39. The results illustrate the opposing effect on cloud forcing within the large-scale circulation; the opposing effects are valid even if we confine the analysis to over warm water.

Another way to examine this relation with respect to large-scale circulation is through the distribution of the remote correlation coefficient. T_s anomalies averaged in an area between 5°N and 5°S and between 170°E and 130°W (shown in Figures 3a and 4a) were correlated with time series of other parameters at all locations. In the surrounding areas to the east, north, and south of this area the correlation between the flux and local T_s anomalies are low, but the remote correlations (not shown) have magnitudes larger than 0.5, supporting the inference of the importance of large-scale circulation.

Plate 6 presents the maps of the remote correlation coefficient between the filtered anomalies of T_s (averaged over the area within the black rectangle) and four parameters, S, E, u, and q_a. To make sure that low-frequency correlations are not masked by high-frequency noise, we attempted to remove the noise by passing the principal components of the anomalies through a low-pass filter and then reconstructing the data field from the filtered components. A seventh-order Butterworth filter [*Oppenheim and Schafer*, 1975] was used, with a cutoff frequency of 2.25 months, a passband tolerance of 1 db for periods longer than 3 months, and a stop band specification that the signal would be reduced by more than 15 db for periods shorter than 2.19 months. Principal component analysis and filtering were performed for the full length of anomalies available for E, S, T_s, u, q_a, and Δq. The patterns of positive and negative correlations for the nonfiltered anomalies (not shown) are the same as those for the filtered anomalies shown in Plate 6. The net effect of filtering is the accentuation of the correlations, particularly in areas outside the equatorial Pacific where the ENSO signal is not so prominent. While filtering distorted the

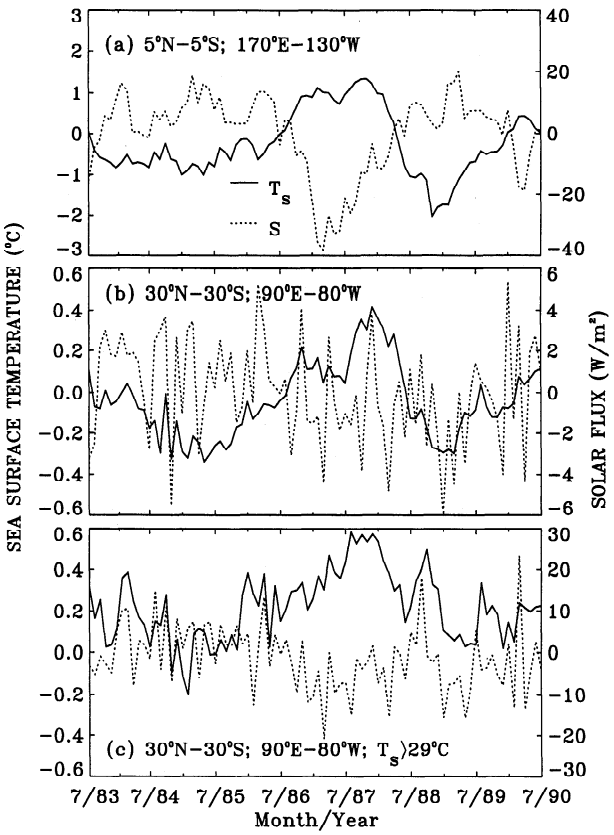

Figure 3. Time series comparison of sea surface temperature and net solar flux anomalies, averaged over various geographical areas and conditions. Locations are (a) 5°N–5°S, 170°E–130°W; (b) 30°N–30°S, 90°E–80°W; (c) 30°N–30°S, 90°E–80°W; $T_s > 29$°C.

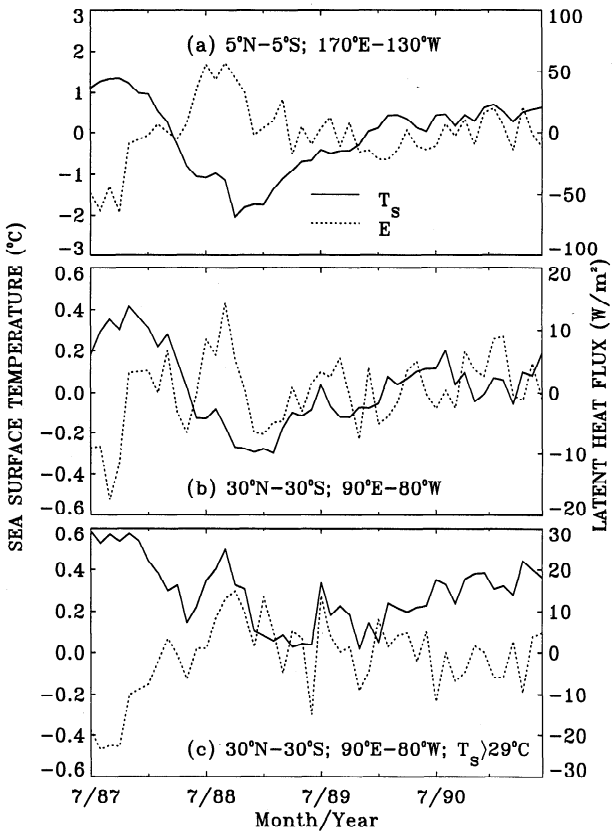

Figure 4. Same as Fig. 8 but for latent heat flux instead of net solar flux.

relative magnitude of the variance, it helped to reveal the low-frequency variations and to interpret the temporal correlations and their distributions. The filtered data are used only to illustrate the relative positions of the positive and negative anomalies.

Similar patterns are found in all the correlations shown in Plate 6. The correlations in the central equatorial Pacific, with a strong extension to the southeast and a weaker extension eastward just north of the equator and with an area of weak or opposite correlation embedded in the east, are surrounded on three sides by areas of opposite correlations. The pattern is associated with dipole oscillation of large-scale convection and circulation as observed by other investigators, particularly in the anomalies of outgoing longwave radiation [e.g., *Lau and Chan*, 1983], with eastward migration of deep convection from the western Pacific, southeast extension of the SPCZ and the equatorward movement of the ITCZ during the warm phase of ENSO, and the reverse during the cold phase. The eastern equatorial Pacific is occupied by dry air; deep convection rarely occurs.

To illustrate the temporal correlations, filtered time series of S and T_s are compared at eight selected locations in Figure 5. At the central equatorial Pacific (Figure 5a) and SPCZ extension (Figure 5b), organized convections were displaced during ENSO. At these locations a warm phase in 1987 corresponds to lower radiative heating and a cold phase in 1988 corresponds to higher radiative heating. Large anomalies in S and strong negative correlation between anomalous S and T_s are found before filtering. Embedded in the region of high negative correlation is a region of low correlation typified by the time series at 5°S and 100°W shown in Figure 5c. In this area the T_s anomaly has similar temporal variation to the immediate surrounding area, but the ENSO signal in S is ill defined. At locations further out (Figures 5d, 5f, 5g, 5h) the phases of T_s anomalies are opposite to that in the central equatorial Pacific, that is, cold during 1987 and warm during 1988. Over the western Pacific, at 5°S and 155°E (Figure 5d), the phase of T_s anomalies is opposite to those in the central Pacific but the phase of S anomalies is the same. The positive local correlation and negative remote correlations reflect the extension of S anomalies eastward of T_s anomalies in the central equatorial Pacific as discussed in section 5. Further to the west, at the equator and 130°E (Figure 5f), the local correlations are negative but the remote correlations are positive. Although T_s anomalies here remain opposite in phase to those in the central equatorial Pacific, the phase of S has changed. The variations at 20°N and 160°E and at 20°S and 160°E (Figures 5g and 5h) are similar to Figure 5f. Further west, in the Arabian Sea, at the equator and 90°E (Figure 5e), the variations are similar to those in the central equatorial Pacific, with a warm phase in 1987 and a cold phase in 1988 but no clear ENSO signal in S.

The filtered anomaly time series of E, T_s, u, and Δq at six locations for the 4-year period are compared in Plate 7. At the equator and 170°W (Plate 7a), typical of the central Pacific, T_s shows a warm phase in 1987 followed by a cold phase in 1988, opposite in phase to E, u, and Δq. At this

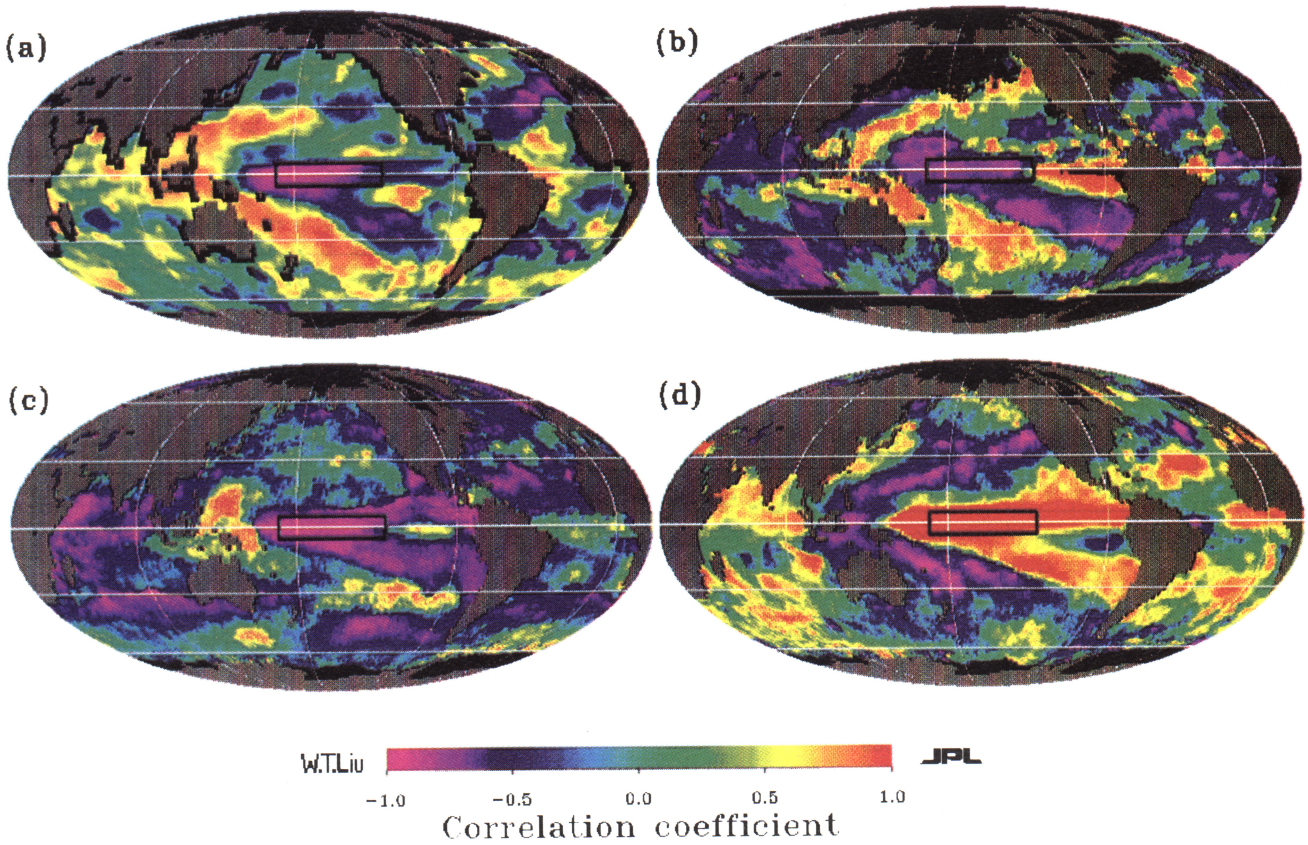

Plate 6. Correlation coefficients between anomalies of sea surface temperature averaged over the area indicated by the black rectangle (5°N to 5°S, 170°E to 130°W) and anomalies of (a) net solar flux; (b) latent heat flux; (c) wind speed; and (d) air humidity. High-frequency variations of the anomalies were filtered out.

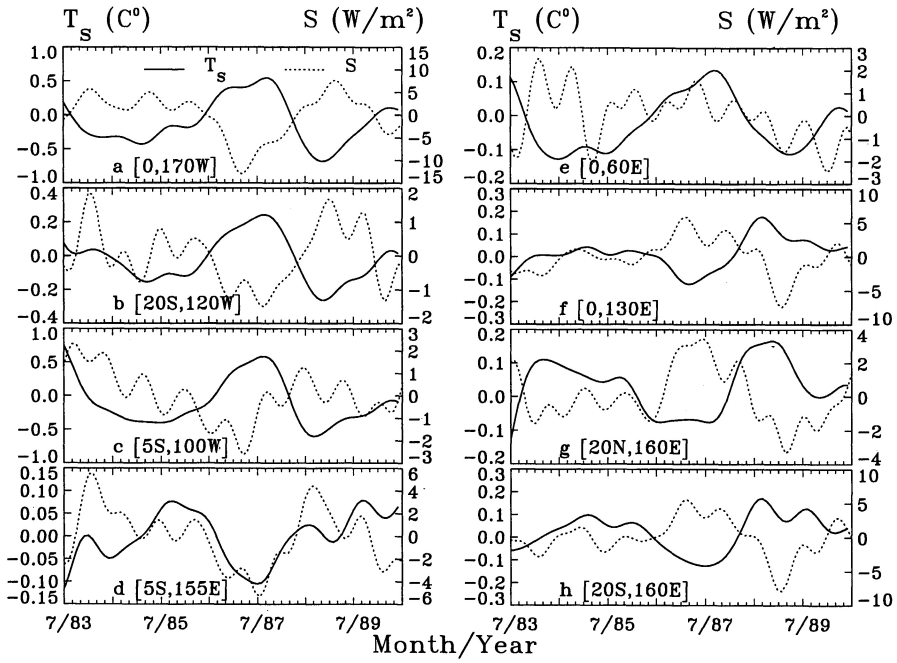

Figure 5. Time series comparison of filtered anomalies of net solar flux and sea surface temperature at (a) 0°, 170°W; (b) 20°S, 120°W; (c) 5°S, 100°W; (d) 5°S, 155°E; (e) 0°, 60°E; (f) 0°, 130°E; (g) 20°N, 160°E; and (h) 20°S, 160°E.

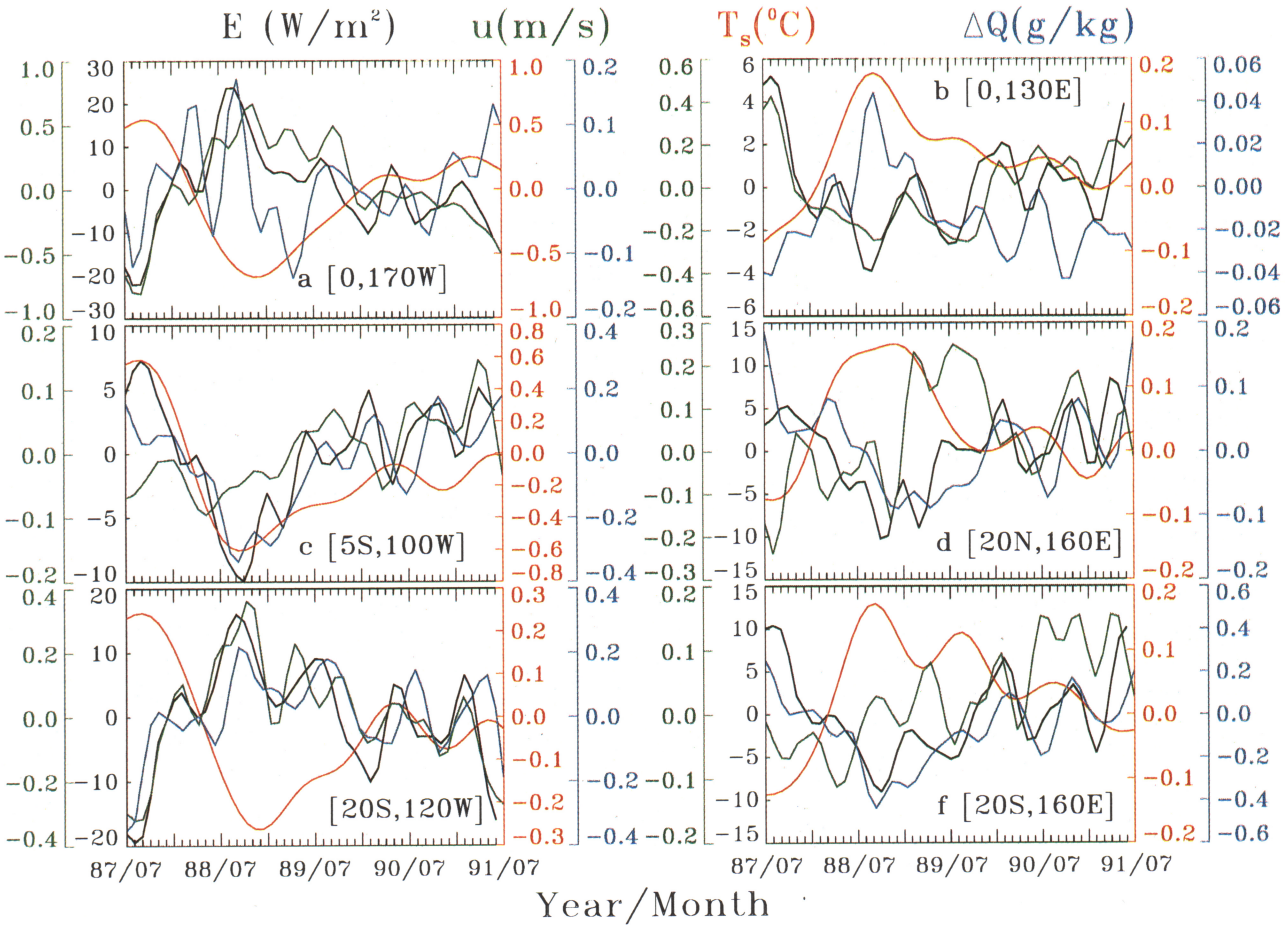

Plate 7. Time series comparison of filtered anomalies of latent heat flux (black line), sea surface temperature (red line), wind speed (green line), and sea-air humidity difference (blue line) at (a) 0°, 170°W; (b) 0°, 130°E; (c) 5°S, 100°W; (d) 20°N, 160°E; (e) 20°S, 120°W; (f) 20°S, 160°E.

location, Δq has the best correlation with E and is likely to be the most influential factor on the anomalous change of E. The variations of SPCZ extension at 20°S and 120°W (Plate 7e) are very similar to those shown in Plate 7a. In the eastern equatorial Pacific, typified by the time series at 5°S and 100°W (Plate 7c), u and q_a anomalies are small, and E anomalies follow the variation of T_s. Surrounding the region of negative remote correlation is the region of positive remote correlation represented by the time series at the three locations on the right side of Plate 7. In the western Pacific at the equator and 130°E (Plate 7b), E correlates best with u and therefore is largely driven by u. In the north at 20°N and 160°E and in the south at 20°S and 160°E the variations of E follow most closely those of Δq. Similar to the seasonal variations discussed in section 7, the anomalies of E are likely to be driven by different factors in different regions affected by large-scale circulations.

8. Discussion and Conclusion

The correlations between the two major surface heat flux components and T_s do not support simple one-dimensional local feedback postulations; the postulations require (1) that T_s is the dominant drive of flux changes and (2) that the fluxes are the most important factors governing T_s changes. The differences in geographical distribution between S and T_s and the lack of negative temporal correlation between them imply that T_s is not the dominant factor in the seasonal variation of local cloud and S; S is mainly changed by the solar incidence angle. However, solar heating is a main factor in the seasonal variation of local T_s except in a zonal belt approximately 5° from the equator where ocean dynamics may play a more important role. For ENSO, S anomalies are not always colocated with T_s anomalies, and negative correlations are present in some but not all of the warm water areas. The lack of positive correlation between anomalies of S and temperature tendency implies that the local effect of anomalous solar heating may not be significant compared with changes in ocean dynamics and other flux components during ENSO. The ubiquitous negative correlations between E and T_s and between E and dT_s/dt, in both monthly means and anomalies, suggest that T_s is not the dominant factor in changing E but imply a possible significant influence of evaporation on upper ocean heat balance and local change of T_s. The results are in agreement with *Liu and Gautier* [1990], who used data from a different time period and derived from different spaceborne sensors.

The results also demonstrate that simple correlation between the flux and T_s may not be sufficient to reveal causality. The negative correlation between E and T_s may be the result of other factors. E is found to be positively

correlated with u and negatively correlated with q_a over most of the ocean. Negative correlation between T_s and u and positive correlation between T_s and q_a result in negative correlation between T_s and E. Over the tropical oceans, ascending air and deep convection overlie warm water and draw surface convergence, which lowers u and raises q_a, or the surface temperature gradient sets up pressure differentials and convergence that facilitate convection [*Lindzen and Nigam*, 1987]; the low E over high T_s is an indirect consequence. The negative correlation may also be the indirect result of ocean dynamics. Stronger wind forcing may change thermocline depth and entrainment intensity and thus upper ocean heat balance.

Although RC found an increase in cloud forcing at the same location as an increase in T_s during ENSO (and their finding is supported by the negative correlations between anomalous T_s and S that we found in the central Pacific), any explanation based on local feedback may not be correct because the increase in cloud forcing is caused by large-scale circulation rather than local T_s. The remote correlations shown in Figure 5 suggest that cloud increase is caused by the shifting of organized convection in the ascending branches of Walker and Hadley circulations which largely overlie warm water. There are areas of equally warm water in the eastern tropical Pacific, but there are no significant S anomalies because atmospheric subsidence prevents high cloud formation. Because of conservation of mass the rising air in convection must be compensated for by subsiding air. When averaged over both the ascending and descending branches of the large-scale circulation, the anomalies of S were found to almost cancel out, despite net changes in T_s anomalies.

High T_s does not necessarily correspond to high E or vice versa; this is true in geographical distribution, in the seasonal changes, and in the ENSO anomalies. The assumptions of constant u and r (see (1)) in the conceptual models of ocean thermostat are spurious. The significance of wind variability over the warm ocean is well documented, both in observation [e.g., *Meyers et al.*, 1986] and in model simulation [e.g., *Seager*, 1989]. The impact of r variability on computation of E was studied by *Liu and Niiler* [1990]. A small error in r or a small percentage error in q_a corresponds to a large percentage error in Δq because q_a is large compared with Δq over warm oceans and E depends linearly on Δq and not q_a. In the tropical oceans it was found that a $\pm 5\%$ error in r causes errors in E that are comparable with the annual and interannual signals. In high latitude ocean, *Liu and Niiler* [1990] also found that the annual cycle of q_a is out of phase with q_s; E (or Δq) therefore leads T_s.

The recent debate on the ocean thermostat addresses global warming, and the analysis were entirely confined to low-frequency variabilities from seasonal to decadal. However, large high-frequency fluctuations have been observed in convection over the warm pool of western Pacific [e.g., *Young et al.*, 1992]. By using monthly mean parameters for estimating latent heat flux with the bulk formula and for computing the correlation coefficient, these high-frequency variances are neglected and erroneous results may be introduced. However, there has been no clear evidence as to any significant long-term and large-scale effects of these short-lived small-scale variances. If the newly installed humidity and radiation sensors in the Tropical Ocean and Global Atmosphere (TOGA) Tropical Atmosphere Ocean (TAO) Array [*McPhaden*, 1993] could provide sufficient accuracy and stability in the long term, temporal multiscale interaction could be examined in the future. The TOGA Coupled Ocean-Atmosphere Response Experiment (COARE) will also provide the observations to understand spatial variation and multiscale processes in the warm pool. It is difficult to separate cause and effect and to isolate the feedback mechanism with available data, as pointed by *Stephens and Slingo* [1992]. This study is only one step toward furthering our understanding of the processes that maintain the warmest sea surface temperature using a unique set of data.

The relation between surface fluxes and T_s is not universal. Neither E nor S alone appear to be sufficient to keep the ocean at an equilibrium temperature. The colocated changes of cloud forcing and T_s observed by RC are likely to be the result of atmospheric circulation (shifting of tropical convective systems) and ocean dynamics (propagation of equatorial waves) during ENSO.

Acknowledgments. This study was performed at the Jet Propulsion Laboratory, California Institute of Technology, under contract with the National Aeronautics and Space Administration (NASA). It was supported by the Interdiscipline Science Investigation of the Earth Observing System and Global Change Data Analysis Program of NASA. The surface solar flux was computed at the Goddard Institute of Space Studies. We are grateful to William Rossow and Rong Fu for their comments and suggestions.

References

Betts, A. K., and W. Ridgway, Climatic equilibrium of the atmospheric convective boundary layer over a tropical ocean, *J. Atmos. Sci.*, *46*, 2621–2641, 1989.

Bishop, J. K. B., and W. B. Rossow, Spatial and temporal variability of global surface solar irradiance, *J. Geophys. Res.*, *96*, 16,839–16,858, 1991.

Bradley, E. F., P. A. Coppin, and J. S. Godfrey, Measurement of sensible and latent heat flux in the western equatorial Pacific Ocean, *J. Geophys. Res.*, *96*, 3375–3389, 1991.

Cayan, D. R., Latent and sensible heat flux anomalies over the northern oceans: Driving the sea surface temperature, *J. Phys. Oceanogr.*, *22*, 859–881, 1992.

Chertock, B., R. Frouin, and R. C. J. Somerville, Global monitoring of net solar irradiance at the ocean surface: Climatological variability and the 1982–1983 El Niño, *J. Clim.*, *4*, 639–650, 1991.

Cornejo-Garrido, A. G., and P. H. Stone, On the heat balance of the Walker circulation, *J. Atmos. Sci.*, *34*, 1155–1162, 1977.

Esbensen, S. K., and R. W. Reynolds, Estimating monthly average air-sea transfer of heat and momentum using the bulk aerodynamic method, *J. Phys. Oceanogr.*, *11*, 457–465, 1981.

Fleagle, R. G., and J. A. Businger, *An Introduction to Atmospheric Physics*, pp. 62–63, Academic, San Diego, Calif., 1963.

Friehe, C. A., and K. F. Schmitt, Parameterization of air-sea interface fluxes of sensible heat and moisture by bulk aerodynamic formulas, *J. Phys. Oceanogr.*, *6*, 801–809, 1976.

Fu, R., A. D. Del Genio, W. B. Rossow, and W. T. Liu, Cirrus-cloud thermostat for tropical sea surface temperatures tested using satellite data, *Nature*, *358*, 394–397, 1992.

Gadgil, S., P. V. Joseph, and N. V. Joshi, Ocean-atmosphere coupling over monsoon regions, *Nature*, *312*, 141–143, 1984.

Godfrey, J. S., and E. J. Lindstrom, The heat budget of the equatorial western Pacific surface mixed layer, *J. Geophys. Res.*, *94*, 8007–8017, 1989.

Graham, N. E., and T. P. Barnett, Sea surface temperature, surface wind divergence, and convection over tropical oceans, *Science*, *238*, 657–659, 1987.

Hsiung, J., Mean surface energy fluxes over the global ocean, *J. Geophys. Res.*, *91*, 10,585–10,606, 1986.

Hsu, S. A., and B. W. Blanchard, The relationship between total precipitable water and surface-level humidity over the sea sur-

face: A further evaluation, *J. Geophys. Res.*, *94*, 14,539–14,545, 1989.

Katsaros, K. B., and J. DeCosmos, Water vapor flux from the sea at high wind speeds, in *Proceedings ICSU/WMO International Symposium on Tropical Cyclone Disasters*, edited by J. Lighthill, Z. Zheng, G. Holland, and K. Emanuel, pp. 386–392, Peking University Press, Beijing, 1993.

Lau, K. M., and P. H. Chan, Short-term climate variability and atmospheric teleconnections from satellite-observed outgoing longwave radiation, I, Simultaneous relationships, *J. Atmos. Sci.*, *40*, 2735–2750, 1983.

Leetmaa, A., The role of local heating in producing temperature variation in the offshore waters of the eastern tropical Pacific, *J. Phys. Oceanogr.*, *13*, 467–473, 1983.

Lindzen, R. S., and S. Niagam, On the role of sea surface temperature gradients in forcing low-level winds and convergence in the tropics, *J. Atmos. Sci.*, *44*, 2418–2436, 1987.

Liu, W. T., Statistical relation between monthly precipitable water and surface-level humidity over global oceans, *Mon. Weather Rev.*, *114*, 1591–1602, 1986.

Liu, W. T., Moisture and latent heat flux variabilities in the tropical Pacific derived from satellite data, *J. Geophys. Res.*, *93*, 6749–6760, 1988.

Liu, W. T., Remote sensing of turbulence flux, in *Surface Waves and Fluxes*, vol. II, edited by G. L. Geenaert and W. J. Plant, pp. 293–309, Kluwer Academic, Norwell, Mass., 1990.

Liu, W. T., and C. Gautier, Thermal forcing on the tropical Pacific from satellite data, *J. Geophys. Res.*, *95*(C8), 13,209–13,217, 13,579–13,580, 1990.

Liu, W. T., and P. P. Niiler, The sensitivity of latent heat flux to the air humidity approximations used in ocean circulation models, *J. Geophys. Res.*, *95*, 9745–9753, 1990.

Liu, W. T., K. B. Katsaros, and J. A. Businger, Bulk Parameterization of air-sea exchanges of heat and water vapor including the molecular constraints at the interface, *J. Atmos. Sci.*, *36*, 1722–1735, 1979.

Liu, W. T., W. Tang, and P. P. Niiler, Humidity profiles over ocean, *J. Clim.*, *4*, 1023–1034, 1991.

Liu, W. T., W. Tang, and F. J. Wentz, Precipitable water and surface humidity over global oceans from SSMI and ECMWF, *J. Geophys. Res.*, *97*, 2251–2264, 1992.

McClain, E. P., W. G. Pichel, and C. C. Walton, Comparative performance of AVHRR-based multichannel sea surface temperatures, *J. Geophys. Res.*, *90*, 11,587–11,601, 1985.

McPhaden, M., TOGA-TAO and the 1991–93 El Niño–Southern Oscillation event, *Oceanography*, *6*, 36–43, 1993.

McPhaden, M., and S. P. Hayes, On the variability of winds, sea surface temperature, and surface layer heat content in the western equatorial Pacific, *J. Geophys. Res.*, *96*, 3331–3342, 1991.

Meyers, G., J. R. Donguy, and R. K. Reed, Evaporative cooling of the western equatorial Pacific Ocean by anomalous winds, *Nature*, *323*, 523–526, 1986.

Newell, R. E., Climate and the ocean, *Am. Sci.*, *67*, 405–416, 1979.

Niiler, P., and J. Stevenson, The heat budget of tropical ocean warm-water pools, *J. Mar. Res.*, *40*, suppl., 465–480, 1982.

Oppenheim, A. V., and R. W. Schafer, *Digital Signal Processing*, pp. 211–218, Prentice-Hall, Englewood Cliffs, N. J., 1975.

Press, W. H., B. P. Flannery, A. Teukolsky, and W. T. Vetterling, *Numerical Recipes*, p. 45, Cambridge University Press, New York, 1989.

Priestley, C. H. B., The limitation of temperature by evaporation in hot climates, *Agric. Meteorol.*, *3*, 241–246, 1966.

Ramanathan, V., and W. Collins, Thermodynamic regulation of ocean warming by cirrus clouds deduced from observations of the 1987 El Niño, *Nature*, *351*, 17–32, 1991.

Ramanathan, V., and W. Collins, Thermostat and global warming, *Nature*, *357*, 649, 1993.

Reynolds, R. W., A real-time global sea surface temperature analysis, *J. Clim.*, *1*, 75–86, 1988.

Rossow, W. B., and R. A. Schiffer, ISCCP cloud data products, *Bull. Am. Meteorol. Soc.*, *72*, 2–20, 1991.

Seager, R., Modeling tropical Pacific sea surface temperature: 1970–87, *J. Phys. Oceanogr.*, *19*, 419–434, 1989.

Stephens, G., and T. Slingo, An air-conditioned greenhouse, *Nature*, *358*, 369–370, 1992.

U.S. Congress, Global change research: The role of clouds in climate change, prepared statement by K. E. Trenberth, hearing before the Committee on Commerce, Science, and Transportation, U.S. Senate, Senate Hearing 102-564, pp. 22–33, 102nd Congress, 1st Session, Oct. 1992.

Waliser, D. E., and N. E. Graham, Convective cloud systems and warm-pool SSTs: Coupled interactions and self-regulation, *J. Geophys. Res.*, *98*, 12,881–12,893, 1993.

Waliser, D. E., N. E. Graham, and C. Gautier, Comparison of the highly reflective cloud and outgoing longwave data sets for use in estimating tropical deep convection, *J. Clim.*, *6*, 331–353, 1993.

Wallace, J. M., Effect of deep convection on the regulation of tropical sea surface temperature, *Nature*, *357*, 230–231, 1992.

Weare, B. C., Interannual variation in net heating at the surface of the tropical Pacific Ocean, *J. Phys. Oceanogr.*, *13*, 873–885, 1983.

Weare, B. C., P. T. Strub, and M. D. Samuel, Marine climate atlas of the tropical pacific ocean, Contribution to *Atmospheric Sci. No. 20*, 147 pp., Univ. of Calif., Davis, 1981.

Young, G. S., D. V. Ledvina, and C. W. Fairall, Influence of precipitating convection on the surface energy budget observed during a tropical ocean global atmosphere pilot cruise in the tropical western Pacific Ocean, *J. Geophys. Res.*, *97*, 9595–9603, 1992.

J. K. Bishop, School of Earth and Ocean Sciences, University of Victoria, Victoria, British Columbia, Canada V8R 3R1.

W. T. Liu and A. Zhang, Jet Propulsion Laboratory, 300–323, California Institute of Technology, Pasadena, CA 91109.

(Received November 29, 1993; revised February 28, 1994; accepted February 28, 1994.)